Analytical Methods

Illustration of the procedure for preparing CFGO and SWCNTs-based electrochemical DNA biosensor
286x266mm (150 x 150 DPI)

Single-walled carbon nanotubes-carboxyl functionalized graphene oxide based

electrochemical DNA biosensor for *thermolabilehemolysin* gene detection

Linlin Yang[a], Xi Li[a]*, Songling Yan[a], Mengmeng Wang[a], Peng Liu[a], Yulin Dong[a], Chaocan

Zhang[b]*

[a]Department of Chemistry, School of Chemistry, Chemical Engineering and Life Science, Wuhan

University of Technology, Wuhan 430070, PR China

[b]School of Materials Science and Engineering, Wuhan University of Technology, Wuhan 430070,

PR China

* Corresponding author.

Tel.: +86 27 87863157; fax: +86 27 87863157

E-mail address: chemlixi@whut.edu.cn (X. Li); polymers@whut.edu.cn (C. Zhang)

Abstract: A sensitive electrochemical DNA biosensor, based on carboxyl functionalized graphene oxide (CFGO) and single-walled carbon nanotubes (SWCNTs) sensing platform and differential pulse voltammetry (DPV) detection, was constructed in this paper. CFGO was prepared via a ring-opening reaction catalyzed by hydrobromic acid and an esterification reaction with oxalic acid, and acted as a mediator for probe DNA (pDNA) immobilization. DNA labeled at 5'-end using amino (NH_2-pDNA) was immobilized on the electrode surface through covalent interaction between amino and carboxyl groups on CFGO. Moreover, single-walled carbon nanotubes (SWCNTs) were employed to improve the electrochemical performance of the biosensor. Based on the different electrochemical responses of $[Fe(CN)_6]^{3-/4-}$ toward pDNA versus double standard DNA after hybridization, the *thermolabilehemolysin* gene sequence could be detected in the concentration range from 1×10^{-6} to 1×10^{-13} mol L^{-1} with a low detection limit of 7.21×10^{-14} mol L^{-1} (at a signal-to-noise ratio of 3). Furthermore, the biosensor also displayed high selectivity to differentiate DNA oligonucleotides from one-base mismatch to noncomplementary. All the reasonable electrochemical performance of the proposed sensing platform indicated that it could be used for the sensitive and accurate determination of other nucleic acids.

Key words: carboxyl functionalized graphene oxide; single-walled carbon nanotube; modified electrode; electrochemical DNA biosensor

1. Introduction

Vibrio parahaemolyticus, a gram-negative bacterium distributed throughout the estuarine environment, is considered as the source of acute gastroenteritis and some cases of septicemia in humans.[1-3] The infection of *Vibrio parahaemolyticus* usually occurs when consuming raw or undercooked seafood.[4] The *thermolabilehemolysin* (*tlh*) gene is considered to be a useful target for the detection of *Vibrio parahaemolyticus* since it was confirmed to exit in all of the *Vibrio parahaemolyticus* stains identified so far.[5] Although conventional methods including enzyme-linked immunosorbant assay (ELISA) and polymerase chain reaction (PCR) are feasible for the detection of *Vibrio parahaemolyticus*,[6-7] the required specialized equipment and time-consuming process made them less suitable for the rapid real-time detection. Compared with these methods, electrochemical biosensors for DNA detection have attracted most of the attention with the advantages of high sensitivity, selectivity, low cost, fast response time, easy handling and portability.[8-9] Generally, the detection process for nucleic acid is completed by the immobilization of probe DNA (pDNA) onto the electrode surface and the examination of electrochemical response before and after the hybridization reaction occurred. The performance of electrochemical DNA biosensors largely depends upon the amount and stability of immobilized pDNA,[10] therefore, a variety of approaches for the fabrication of DNA biosensors have been reported using bioelectrodes based on various modified materials including nanostructure, metals and metal oxides, polymers etc[11] since the bare electrodes are limited in pDNA immobilization.

As a two dimensional sheet of sp^2 bonded carbon atomics, graphene (GR) has attracted increasing attention on account of its remarkable electronic and mechanical properties, such as extreme high surface area, excellent electrochemical conductivity, enhanced electron transfer

kinetics, good biocompatibility and high mechanical strength.[12-15] The aromatic regions of GR can

also offer active sites to interact with other aromatic molecules through π-π supramolecular

interactions.[16] Therefore, GR hold great promise for potential applications in various areas.

Electrochemical biosensors with satisfactory sensitivity and selectivity based on GR-based

materials have also been reported in recent years.[17-19] However, the present GR possesses the

defect of forming irreversible agglomerates through the van der Waals interaction and π stacking,

which greatly restricts its further application in electrochemical sensing.[20] Thus, graphene oxide

(GO) is introduced because of its enhanced solubility and dispersion ability caused by abundant

oxygen functional groups such as epoxy, hydroxyl, peroxy, carbonyl and carboxyl groups

decorated on the basal planes and edges.[21] Whereas, GO can also be utilized for pDNA covalent

immobilization through amidation between its carboxyl groups and amino labeled on the 5'-end of

probe. For the purpose of providing more anchor for pDNA immobilization, carboxyl

functionalized GO (CFGO) have been designed to increase the density of carboxyl groups.[22]

Shiddiky reported an epithelial cell adhesion molecule (EpCAM) electrochemical immunosensor,

carboxylated graphene oxide nanosheets was presented as a mediator for the link of streptavidin

and amine-functionlized QDs to form signal-transduction labels.[23] Yuan fabricated a novel

carboxyl functionalized graphene oxide-gold nanoparticles modified glassy carbon electrode

(GCE) for the detection of thrombin with a reasonable detection limit.[24] Most of the presented

carboxylation methods are based on the interaction with chloroacetic acid under strongly basic

conditions. In this work, CFGO was fabricated through a ring-opening reaction with hydrobromic

acid and an esterification reaction with oxalic acid. Hydrobromic acid was employed to convert

the epoxide groups (–O–) on the basal plane of GO into hydroxyl groups (–OH) and oxalic acid

was introduced to interact with the –OH groups. Both the edged carboxyl groups and the basal

oxygenated groups could be taken advantage after the carboxylation process. As far as we

concerned, this method has not been utilized in the fabrication of electrochemical DNA biosensors.

The increased oxygen content after carboxylation resulted in the rise of hydrophilia of CFGO,

however, it also led to the decrease in electric conduction ability. Carbon nanotubes (CNTs) has

emerged as a promising class of materials in constructing electrochemical DNA biosensors to

accelerate electric-transfer and enhance the electrical signals based on their unique merits,[25-27]

such as superb electrocatalytic activity, large surface area, and high stability.[28-30] Wang et al.

found that $[Fe(CN)_6]^{3-/4-}$ at a FePt nanoparticles and double-walled carbon nanotubes (FePt-CNTs)

modified GCE exhibited a higher and sharper oxidation peak compared to that of the bare GCE

and FePt modified GCE.[31] For the interfacial electron-transfer resistance (R_{et}) value, the

FePt-CNTs modified GCE was 275 Ω smaller than that of the FePt modified electrode. The

composite materials of reduced graphene oxide-carbon nanotubes developed by Sharma[16]

performed maximum current signal in cyclic voltammogram scans on the surface of screen print

electrode (SPE), compared with the CNTs or rGO modified SPE. The hybridization of GO and

CNTs was expected to have synergistic effects as they have similar structural and physical

properties.[32] Considering those impacts, single-walled carbon nanotubes (SWCNTs) was adopt to

enhance the electrode surface area and charge-transfer rate before the CFGO was added.

To sum up, in this work, CFGO with a novel preparation method was utilized as a mediator

for 5'-end amino modified pDNA immobilization. SWCNTs were employed to promote the

electric transfer and amplify the detectable electrochemical signals. After the target DNA

hybridized with pDNA to form a double helix structure on the electrode surface, the

electrochemical response of $[Fe(CN)_6]^{3-/4-}$ decreased, providing the possibility to acted as electrochemical indicator for DNA detection. The prepared electrochemical DNA biosensor was utilized as a platform for capturing the *tlh* gene sequence. Low detection limit was achieved under the optimal experimental conditions.

2. Experimental

2.1. Apparatus

All electrochemical measurements were performed using a CHI 660D electrochemical workstation (Shanghai Chenhua Equipments, China) with a conventional three-electrode system consisted of a bare or a modified GCE as the working electrode, a platinum wire as the counter electrode, and a saturated calomel electrode (SCE) as the reference electrode. Fourier Transform Infrared Spectroscopy (FT-IR) was recorded in a range of wave numbers from 4000 to 500 cm^{-1} with a Nexus (Thermo Nicolet, USA) FT-IR spectrometer. The variation in content of oxygen containing functional groups before and after the carboxylation of GO were estimated by X-ray photoelectron spectroscopy (XPS) using a VG Multilab 2000 spectrometer (Thermo, VG Multilab 2000, USA) using Al (300W) radiation (hv=15 eV). The morphology of different modified electrodes was investigated by field emission scanning electron microscope (SEM) (Zeiss Ultra Plus, Germany).

2.2. Reagents

The SWCNTs with less than 2 nm in diameter and 5–15 μm in length was purchased from

Shenzhen Nanotech Port Co., Ltd (Shenzhen, China). The SWCNTs suspension (0.1 mg mL^{-1})

was prepared as described previously.[33]

Synthetic oligonucleotides, which were selected from *tlh* gene sequence, were purchased

from Shanghai Sangon Biological Engineering Tech. Ltd. Co. (China) and used without further

purification. The 23-base sequences for probe, target, one-base mismatch, three-base mismatch

and non-complementary were the following:

probe DNA: 5'-NH$_2$-GATGACACTGCCAGATGCGACGA-3';

target DNA: 5'-TCGTCGCATCTGGCAGTGTCATC-3';

one-base mismatch DNA: 5'-TCGTCGCATCTAGCAGTGTCATC-3';

three-base mismatch DNA: 5'-TAGTCGCATCTAGCAGTGTCAGC-3';

non-complementary DNA: 5'-ATCCTTTGCAATTGCCCAGTCGG-3'.

The phosphate buffer solution (PBS) of 50 mmol L^{-1} (pH=7.0) were prepared by a certain

percentage of the mixture solution of Na$_2$HPO$_4$ and NaH$_2$PO$_4$. All oligonucleotides were dissolved

in 50 mmol L^{-1} PBS (pH=7.0) with 0.1 mol L^{-1} NaCl and were kept in frozen.

Flaked graphite was purchased from Nanjing xianfeng nano Co. (Nanjing, China).

N-(3-dimethyl-amino-propyl)-N'-ethylcarbodiimide   hydrochloride   (EDC)   and

N-hydroxy-succinimide (NHS) were obtained from Shanghai Yuanye Biotechnology Co., Ltd

(Shanghai, China). Sodium dodecyl sulphate (SDS), HBr, C$_2$H$_2$O$_4$, KCl, Na$_2$HPO$_4$, NaH$_2$PO$_4$,

K$_3$Fe(CN)$_6$, K$_4$Fe(CN)$_6$ and other common reagents, were of analytical grade or higher and

purchased from Sinopharm Chemical Reagent Co., Ltd (Shanghai, China). All the reagents were

used as received and aqueous solutions were prepared with double distilled water.

2.3. Synthesis of the CFGO

GO was synthesized from graphite according to the modified Hummer's method.[34] CFGO

was synthesized as previously described.[35] Briefly, 5.0 mL HBr was added into 30.0 mL of 2.5

mg mL^{-1} GO solution, and the mixture was vigorously stirred for 12 h. Then 1.50 g oxalic acid

was added and stirred for 4 h. The resulted CFGO solution was repeatedly washed with double

distilled water and dried at 50℃ in vacuum for about 24 h. The CFGO was dispersed in water by

ultrasonication to form aqueous solution (0.25 mg mL^{-1}, 30 mL).

2.4. Fabrication of CFGO/SWCNTs/GCE

Prior to modification, GCE was mechanically polished with 1.0 μm and 0.3 μm alumina

slurry to a mirror-like surface. Then it was rinsed ultrasonically with acetone and double distilled

water successively. Cyclic voltammetry (CV) in a 0.5 mol L^{-1} sulfuric acid solution was used to

provide an electrochemically clean for GCE to remove any adsorbed residual impurities. A fresh

cleaned GCE was treated by dripping 5 μL of 0.1 mg mL^{-1} SWCNTs and then dried in air at room

temperature to fabricate a SWCNTs modified GCE (SWCNTs/GCE). Finally,

CFGO/SWCNTs/GCE was accomplished by dropping 5 μL of 0.25 mg mL^{-1} CFGO onto the

SWCNTs/GCE surface and dried to allow the formation of hybridized thin film.

2.5. Immobilization and hybridization

Immobilization of probe DNA on the CFGO/SWCNTs/GCE surface was accomplished through covalent bonding between amino groups of the probe and the carboxyl groups of CFGO. Firstly, the CFGO/SWCNTs/GCE was immersed into a mixture solution containing 400 mmol L^{-1} EDC and 100 mmol L^{-1} NHS for a certain time to activate the carboxyl groups, followed by dropping 5 μL of 1×10^{-6} mol L^{-1} probe DNA onto the electrode surface. The probe DNA modified electrode should be washed with 0.5% SDS solution and double distilled water extensively to remove the unbounded oligonucleotides after incubated at 4℃ for a period of time. The obtained electrode was denoted as pDNA/CFGO/SWCNTs/GCE.

Hybridization was performed by dropping 5.0 μL of hybridization solutions that contained certain concentration of target DNA or complementary DNA with different mismatch degrees onto the pDNA/CFGO/SWCNTs/GCE. After that, the obtained electrode was rinsed thoroughly with 0.5% SDS solution and double distilled water respectively to wash off the unhybridized DNA.

2.6. Electrochemical detection

The cyclic voltammograms (CVs) were recorded in 0.1 mol L^{-1} KCl solution containing 5.0 mmol L^{-1} $[Fe(CN)_6]^{3-/4-}$ (1:1) in a potential scanning range from + 0.6 to − 0.3 V with a scan rate of 100 mV s^{-1}. Differential pulse voltammetry (DPV) measurement was carried out in the same supporting electrolyte and potential range above with the pulse amplitude 0.05 V, pulse width 0.2 s, and the pulse period 0.5 s. Analyses were always made in triplicate.

3. Results and discussion

3.1. Morphology and structure characterizations of CFGO

FT-IR spectroscopy were applied to verify the formation of oxygen functional groups from GO to CFGO (Fig. 1). In the FT-IR spectrum of GO, the characteristic absorption peaks in 1730 and 1624 cm^{-1} could be attributed to C=O stretching of carboxyl groups and C=C stretching vibration of aromatic rings respectively.[35-36] In addition, the absorption bands of 3430 and 1374-1051 cm^{-1} showed the presence of –OH and the C-O stretching of the C-OH/C-O-C groups, respectively.[35] As for the spectrum of CFGO, the enhanced absorption peaks of C=O and –OH (1730 and 3430 cm^{-1}) confirmed the presence of increased amount of carboxyl groups on CFGO.
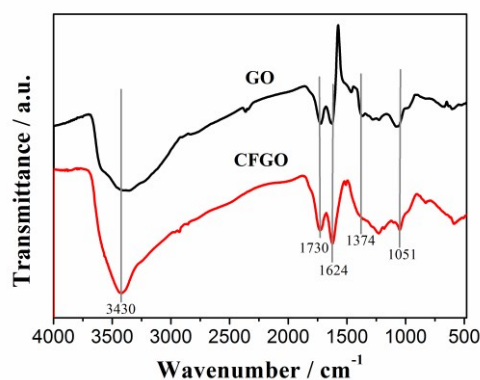

Figure 1. FTIR spectra of GO and CFGO

XPS characterizations were carried out to gain more insights into the variations of the oxygen-containing functional groups in GO and CFGO. As shown in Fig. 2, the C_{1s} XPS spectrum containing three main types of carbon bonds that could be identified at 284.6 (C=C), 286.39 (C=O), and 288.6 eV (O-C=O).[36-37] Treatment of GO with HBr and oxalic acid provided CFGO with an increase of oxygen functionalities and a decreased C/O ratio from 3.07 to 2.35 in the XPS survey scans. Compared to that of GO, the percentage distribution of C=O and O-C=O in CFGO

increased by 0.3 and 7.4% respectively, which could be strongly signified the successful
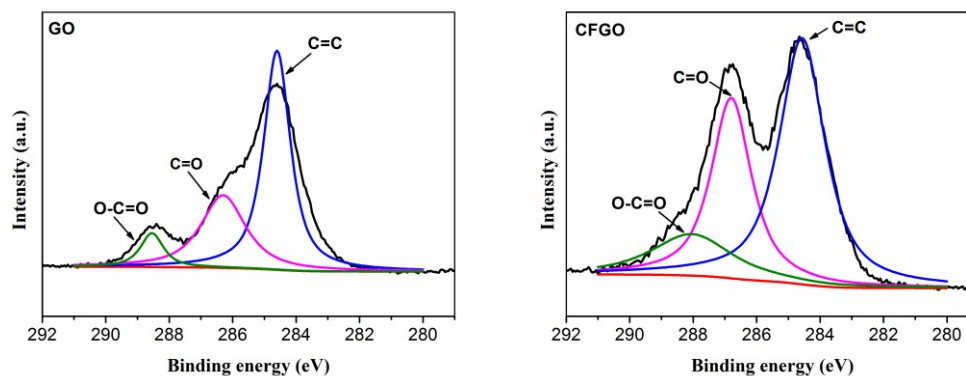
carboxylation of GO.

Figure 2. C1s XPS spectra of GO and CFGO

The morphologies of the as-prepared SWCNTs/GCE and CFGO/SWCNTs/GCE were

characterized by SEM. As shown in Fig. 3 (a), SWCNTs distributed onto the electrode surface and

formed a three-dimensional network structure. After the addition of CFGO (Fig. 3(b)), the outline

of the network structure was obscured and few-layer flexible wrinkled sheets of CFGO was

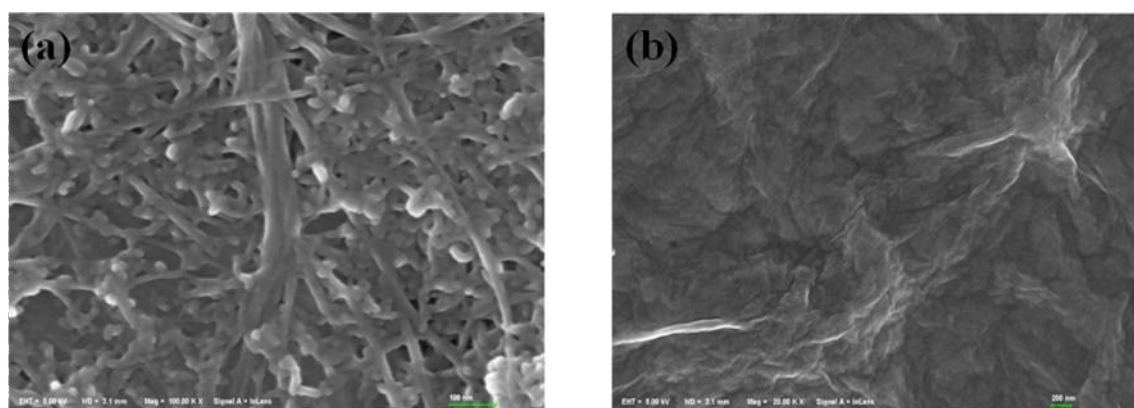revealed, indicated that the CFGO had been deposited onto the SWCNTs/GCE successfully.

Figure 3. SEM image of SWCNTs/GCE (a) and CFGO/SWCNTs/GCE (b)
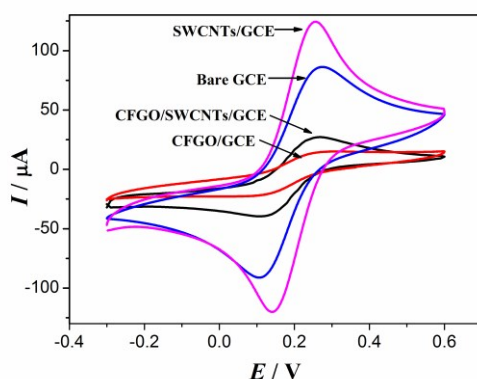
3.2. Electrochemical characterization of modified electrodes

Figure 4. CVs of 5.0 mmol L^{-1} $K_3[Fe(CN)_6]$/$K_4[Fe(CN)_6]$ including 0.1 mol L^{-1} KCl at a bare GCE, CFGO/GCE,

SWCNTs/GCE and CFGO/SWCNTs/GCE.

In order to investigate the electrochemical properties of different modified electrodes and the

synergistic effects between CFGO and SWCNTs on GCE surface, CV was carried out and shown

in Fig. 4. A pair of well-defined redox peaks corresponding to the electrochemical response of

$[Fe(CN)_6]^{3-/4-}$ coupled with the bare GCE was clearly observed. After SWCNTs added onto the

bare GCE, the current response became greater with a smaller peak-to-peak separation (ΔE_P). This

phenomenon could be the distinct evidence of the fact that SWCNTs could promote the electric

transfer greatly. When the GCE was coated with CFGO, the peak currents of $[Fe(CN)_6]^{3-/4-}$

decreased greatly which suggested that the electron transfer of $[Fe(CN)_6]^{3-/4-}$ was hindered by the

assemblage of CFGO thin film. While after functionalized with SWCNTs, the prepared

CFGO/SWCNTs/GCE exhibited dramatically increasing redox peak currents. This phenomenon

might be attributable to the unique electronic structures and electrochemical properties of

SWCNTs which had enhanced the electrochemical activity of electrode.

The specific surface area of SWCNTs/GCE was determined by CVs in 5.0 mmol Ł$^{-1}$

K$_3$[Fe(CN)$_6$]/K$_4$[Fe(CN)$_6$] including 0.1 mol L^{-1} KCl at different scan rates (v). According to the

Randles-Sevcik equation (1):

$$I_P = 2.69 \times 10^5 A \times D^{1/2} n^{2/3} C v^{1/2}, \quad (1)$$

The obtained electroactive surface of SWCNTs/GCE was 0.094 cm^2, which was larger than
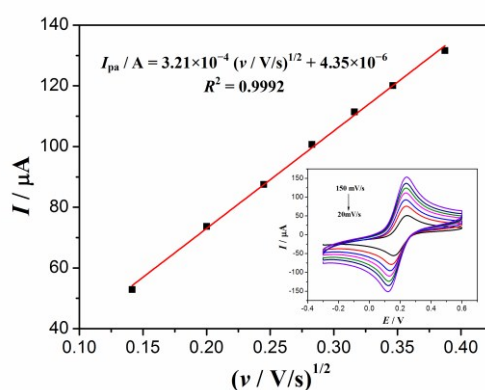
that of the bare GCE (about 0.05 cm^2).

Figure 5. Electroactive surface area of SWCNTs/GCE by CVs in 5.0 mmol Ł$^{-1}$ K$_3$[Fe(CN)$_6$]/K$_4$[Fe(CN)$_6$]

containing 0.1 mol Ł$^{-1}$ KCl at different scan rates (20, 40, 60, 80, 100, 120, 150 mV s^{-1}).

Compared with CV, which expressed well to observe redox peaks, DPV performed a

higher sensitivity and resolution in the detection of peak currents. Therefore, DPV was employed

in the DNA detection. [Fe(CN)$_6$]$^{3-/4-}$ was often employed as electrolyte in electrochemical

impedance biosensors. It had been well demonstrated that [Fe(CN)$_6$]$^{3-/4-}$ also could be used as

indicator according to the different electrochemical responses before and after DNA hybridization.

The DPV curves of [Fe(CN)$_6$]$^{3-/4-}$ at CFGO/SWCNTs/GCE, pDNA/CFGO/SWCNTs/GCE and

after target DNA hybridization were displayed in Fig. 6. The peak current of [Fe(CN)$_6$]$^{3-/4-}$

belonging to pDNA/CFGO/SWCNTs/GCE decreased because probes immobilized on the

electrode surface prevented the ion exchanges between the solution species and electrode in the

redox reaction procedure.[38] A noticeable current decrease was obtained after interacted with target

DNA, since the negatively charged $[Fe(CN)_6]^{3-/4-}$ molecules were repelled by the negatively

charged phosphate backbone of double-standard DNA. The difference in the peak currents of

$[Fe(CN)_6]^{3-/4-}$ in pDNA/CFGO/SWCNTs/GCE and after hybrid formation proved that

$[Fe(CN)_6]^{3-/4-}$ could be used as an effective indicator for the determination of DNA hybridization.

Compared with the pDNA/GCE (showed a peak current of 36.32 μA, not shown in this figure),

the change of the redox peak current value of $[Fe(CN)_6]^{3-/4-}$ on the pDNA/CFGO/SWCNTs/GCE

was much larger. This indicated the higher electrochemical properties and larger surface area of

SWCNTs played an important role in enhancing the electric signal, and the addition of CFGO

contributed in effective immobilization of pDNA, which were the key factors to improve the

sensitivity of the electrochemical DNA biosensor.
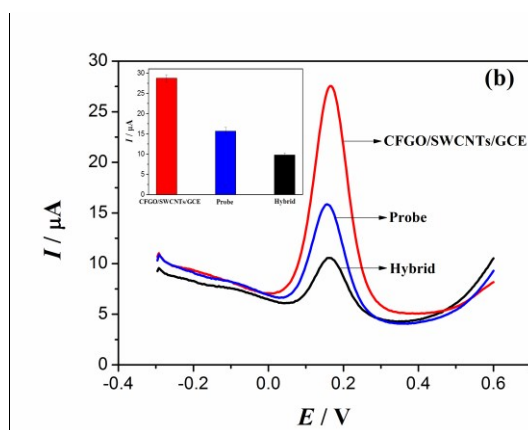
Figure 6. DPV peak currents of CFGO/SWCNTs/GCE, pDNA/CFGO/SWCNTs/GCE (Probe) and after

hybridization with target DNA (Hybrid) in the same electrolyte solution.

3.3. Optimization of experimental conditions

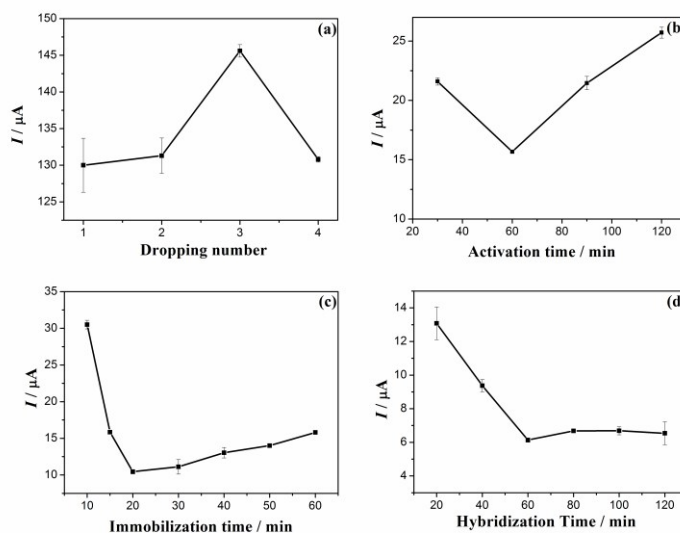**Figure 7.** The dependence of peak currents of $[Fe(CN)_6]^{3-/4-}$ in 5.0 mmol L^{-1} $K_3[Fe(CN)_6]$/$K_4[Fe(CN)_6]$ solution containing 0.1 mol L^{-1} KCl at the different modified GCE on the amount of SWCNTs (a), activation time of carboxyl on CFGO (b), the immobilization time of probe DNA (c) and the hybridization time of target DNA (d).

We investigated the effects of the SWCNTs amount, the activation time of carboxyl groups in CFGO, the immobilization time of probe DNA and the hybridization time of target DNA on the performance of the biosensor. Fig. 7 showed the peak currents of $[Fe(CN)_6]^{3-/4-}$ in CV curves on various modified electrodes.

The effect of SWCNTs amount was investigated by dropping 5 μL of the SWCNTs suspension (0.1 mg mL^{-1}) many times on GCE surface. The relationship between the oxidation peak current and dropping numbers was shown in Fig. 7(a). With the increase of dropping numbers from 1 to 4, the peak currents exhibited an enhancement effect and reached the maximal when dropping 3 times. Thus 3 was selected as the dropping numbers for the preparation of CFGO/SWCNTs/GCE.

The activation time was optimized for the activation of carboxyl groups. Fig. 7(b) proved the electric response of pDNA/CFGO/SWCNTs/GCE versus activation time. As shown in this figure, the oxidation peak current achieved the minimum at 60 min, which meant that the activated available carboxyl groups on CFGO had attained the maximum number at this period, and the surface of the modified electrode would be saturated of probe. The increase of electrical signals after 60 min might be ascribed to the generation of byproducts caused by too long activation time. Thus, 60 min was adequate for activation of the CFGO/SWCNTs/GCE surface.

The influence of immobilization time for probe DNA and hybridization time for target DNA were also studied. As shown in Fig. 7(c), the redox peak currents of $[Fe(CN)_6]^{3-/4-}$ decreased as the immobilization time dragged on, indicating the amount of adsorbed probe DNA on the activated CFGO/SWCNTs/GCE increased and saturated at approximately 20 min. Fig. 7(d) performed a decreased electric signal of $[Fe(CN)_6]^{3-/4-}$ with increasing hybridization time from 20 to 60 min, which could attribute to the raising negative charge caused by the formation of more and more double helix structure. The hybridization reaction was accomplished during 60 min because it maintained stability after 60 min. Thus, the immobilization time of 20 min and the hybridization time of 60 min were chosen in subsequent experiments.

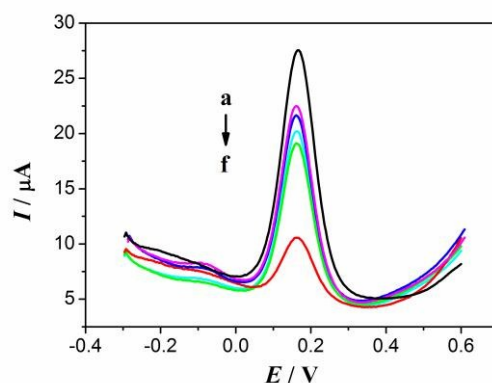**3.4. Selectivity and sensitivity of the electrochemical DNA biosensor**

Figure 8. Differential pulse voltammograms of $[Fe(CN)_6]^{3-/4-}$ at CFGO/SWCNTs/GCE (a), pDNA/CFGO/

SWCNTs/GCE (b) and after hybridized with 1×10^{-6} mol L^{-1} target DNA sequence (f), one-base mismatch DNA

sequence (e), three-base mismatch DNA sequence (d) and noncomplementary DNA sequence (c).

Under the optimal experimental conditions, control experiments were carried out to assess

whether the biosensor responded selectively to target DNA. Probe/target DNA, probe/one-base

mismatch, probe/three-base mismatch and probe/non-complementary couples were prepared in a

concentration of 1×10^{-6} mol L^{-1} to inspect the selectivity of the biosensor (Fig. 8). As expected,

the lowest peak current of $[Fe(CN)_6]^{3-/4-}$ was observed for the pDNA/CFGO/SWCNTs/GCE

hybridization with target DNA (curve f), suggesting the successfully formation of double-standard

DNA increasing the electrostatic repulsion interaction to $[Fe(CN)_6]^{3-/4-}$ on the electrode surface.

After hybridized with one-base mismatch DNA sequence (curve e) or three-base mismatch DNA

sequence (curve d), significant increased electrochemical response was obtained as compared with

the target DNA, indicating the complete hybridization was not accomplished because of the base

mismatch. After the non-complementary DNA sequence was hybridized (curve c), the change in

electric signal of $[Fe(CN)_6]^{3-/4-}$ was little compared to that of pDNA/CFGO/SWCNTs/GCE

(curve b), meant that the hybridization reaction was not happen for this oligonucleotides due to the

sequence mismatching. The slight decrease on the peak current might be owned to the

non-specific adsorption of DNA on the electrode surface. Moreover, the DPV signals for

non-complementary sequence, three-base match sequence, one-base mismatch sequence and target

DNA were decreased in turn, demonstrating that the electrochemical DNA biosensor showed high

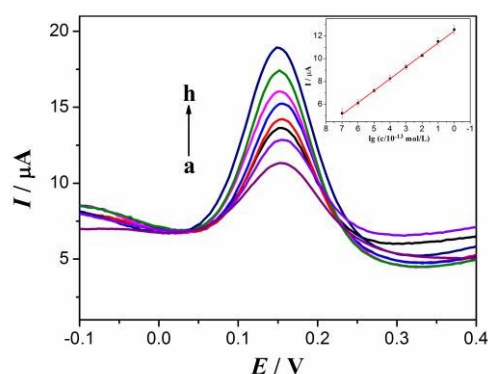selectivity and efficiency for the detection of DNA hybridization.

Figure 9. DPVs of 5 mmol L^{-1} $K_3[Fe(CN)_6]/K_4[Fe(CN)_6]$ on pDNA/CFGO/SWCNTs/GCE after hybridization

with different concentrations of target DNA sequence (from a to h were 1×10^{-6} mol L^{-1}, 1×10^{-7} mol L^{-1}, 1×10^{-8}

mol L^{-1}, 1×10^{-9} mol L^{-1}, 1×10^{-10} mol L^{-1}, 1×10^{-11} mol L^{-1}, 1×10^{-12} mol L^{-1} and 1×10^{-13} mol L^{-1} respectively).

Inset showed the plots of peak current versus the logarithm of target DNA concentration.

In Fig. 9, the DPVs for target DNA oligonucleotides in the concentration range of 1×10^{-6}

mol L^{-1} to 1×10^{-13} mol L^{-1} were performed to investigated the sensitivity of the DNA biosensor.

The obtained redox peak currents of $[Fe(CN)_6]^{3-/4-}$ after hybridization were recorded. It could be

seen that the peak current of $[Fe(CN)_6]^{3-/4-}$ gradually increased as the concentration target DNA

decreased, demonstrating that the amount of DNA duplex at the CFGO/SWCNTs/GCE surface

decreased during the hybridization reaction. The relationship of DPV response with the logarithm

of target DNA concentration could be plotted with the regression equation of (2)

$$I_P \text{ (μA)} = 12.426 - 1.044\log (c/10^{-13} \text{ mol } L^{-1}), R^2 = 0.999 \text{ (inset in Fig. 9)}, \quad (2)$$

The detection limit was obtained as 7.21×10^{-14} mol L^{-1} (S/N=3). A comparison between the developed biosensor and previously reported assays with similar modified electrodes was summarized in Table 1.[39-45] Obviously, the present biosensor exhibited a wider linear range and a reasonable detection limit compared to most of others. Although some biosensors provided wider linear concentration range or lower detection limit, their preparation were complicated,[41, 44] and some of the modified materials were very expensive.[42, 43]

Table 1 The comparison of experiment results in the determination of DNA hybridization with different modified electrodes.

Modified Electrode[a]	Linear range (mol L^{-1})	Determination limit (mol L^{-1})	Determination method	References
PTCA/GR	10^{-12}-10^{-6}	5.0×10^{-13}	EIS	39
Carbon nanofibre/chitosan layer/GCE	5×10^{-10}-4×10^{-8}	8.8×10^{-11}	DPV	40
ssDNA-probe-wrapped-SWCNTs/GCE	10^{-11}-5×10^{-9}	10^{-12}	SWV	41
Fe@AuNPs-AETGO/GCE	10^{-14}-10^{-8}	2.0×10^{-15}	SWV	42
AuNPs-ATPGO/GCE	10^{-13}-10^{-9}	1.13×10^{-14}	EIS	43
PDDA/PDC-SWNTs/GCE	10^{-11}-10^{-6}	2.6×10^{-12}	DPV	44
GR-PBA/Au electrode	10^{-15}-5×10^{-12}	3.8×10^{-16}	DPV	45
CFGO/SWCNTs/GCE	10^{-13}-10^{-6}	7.27×10^{-14}	DPV	This work

[a] PTCA: 3,4,9,10-perylene tetracarboxylic acid; GR: graphene; AuNPs: gold nanoparticles; AETGO: 2-aminoethanethiol functionalized graphene oxide; ATPGO: paminothiophenol functionalized graphene oxide; PDDA: poly(diallyldimethyl ammonium chloride); PDC: 2,6-Pyridinedicarboxylic acid; PBA: pyrenebutyric acid

3.5. Reproducibility and stability of the electrochemical DNA sensor

The reproducibility of the DNA sensor was investigated by five parallel electrochemical measurements for 1×10^{-6} mol L^{-1} and 1×10^{-8} mol L^{-1} target DNA, respectively. A relative standard deviation (RSD) of 3.27% and 2.48% were estimated in this experiment, exhibiting a high reproducibility of the proposed electrochemical DNA biosensor.

The stability of the as-prepared DNA biosensor was also studied. No obvious current changes were found in its CV curves after a continuous scanning on CFGO/SWCNTs/GCE for twenty times, indicated the high stability of this modified electrode caused by π-π stacking between each modified material and GCE surface.

A continuous scanning on pDNA/CFGO/SWCNTs/GCE for ten times in 5.0 mmol L^{-1} $[Fe(CN)_6]^{3-/4-}$ solution was carried out with a RSD of 0.27%. Furthermore, the pDNA/CFGO/SWCNTs/GCE was placed in PBS for 5 h, and measured in 5.0 mmol L^{-1} $[Fe(CN)_6]^{3-/4-}$ solution containing 0.1 mol L^{-1} KCl by DPV. The current responses obtained at the electrode incubated in PBS and unincubated respectively showed no characteristic changes (ΔI_P = 1.01 μA). Those results illustrated that the pDNA/CFGO/SWCNTs/GCE maintained good stability.

Conclusion

In this work, we demonstrated a novel strategy for the carboxylation of GO by the oxidation of hydrobromic acid and esterification of oxide acid, and first employed it into the fabrication of electrochemical DNA biosensor for the detection of *tlh* gene sequence related to *Vibrio parahaemolyticus*. CFGO acted as a mediator for probe DNA immobilization. The introduction of SWCNTs increased the electrode surface area to support a much higher loading amount of probe and therefore enhancing the electrochemical signal and sensitivity of the biosensor. Under the

optimal working conditions, this biosensor could detect target DNA down to 7.27×10^{-14} mol L^{-1} with a detectable concentration range from 1×10^{-6} to 1×10^{-13} mol L^{-1}. A high selectivity to one-base mismatch, three-base mismatch and non-complementary DNA sequences was also obtained. Therefore, the proposed approach provided a universal platform for genetic target analysis in biomedical and bioanalytical application.

Acknowledgements

Reference

1. M. B. Lan, Q. Zhou and Y. H. Zhao, *Science China Chemistry*, 2010, 53, 1366-1370.

2. L. N. Ward and A. K. Bej, *Applied and environmental microbiology*, 2006, 72, 2031-2042.

3. C. A. Broberg, T. J. Calder and K. Orth, *Microbes and Infection*, 2011, 13, 992-1001.

4. B. L. Sarkar, G. B. Nair and B. K. Sircar, *Applied and environmental microbiology*, 1983, 46, 288-290.

5. P. S. M. Yeung and K. J. Boor, *Foodborne Pathogens & Disease*, 2004, 1, 74-88.

6. T. Honda, T. Miwatani, Y. Yabushita, N. Koike, K. Okada, *Clinical and Vaccine Immunology*, 1995, 2, 177-181.

7. Y. B. Kim, J. Okuda, C. Matsumoto, N. Takahashi, S. Hashimoto and M. Nishibuchi, *J Clin Microbiol*, 1999, 37, 1173-1177.

8. S. Laschi, R. Miranda-Castro and E. González-Fernández, *Electrophoresis*, 2010, 31, 3727-3736.

9. G. Bagni, D. Osella and E. Sturchio, *Analytica chimica acta*, 2006, 573, 81-89.

10. L. Lu, L. Xu and T. Kang, *Applied Surface Science*, 2013, 284, 258-262.

11. M. Tak, V. Gupta and M. Tomar, *Biosensors and Bioelectronics*, 2014, 59, 200-207.

12. C. Lee, X. Wei and J. W. Kysar, *Science*, 2008, 321, 385-388.

13. X. Li, Y. Zhu and W. Cai, *Nano letters*, 2009, 9, 4359-4363.

14. T. Tian, Z. Li and E. C. Lee, *Biosensors and Bioelectronics*, 2014, 53, 336-339.

15. M. Pumera, A. Ambrosi and A. Bonanni, *TrAC Trends in Analytical Chemistry*, 2010, 29, 954-965.

16. P. Sharma, V. Bhalla and V. Dravid, *Scientific reports*, 2012, 2, DOI: .

17. G. Yang, J. Cao and L. Li, *Carbon*, 2013, 51, 124-133.

18. T. Mondal, A. K. Bhowmick and R. Krishnamoorti, *Journal of Materials Chemistry*, 2012, 22, 224811-22487.

19. M. Zhou, Y. Wang and Y. Zhai, *Chemistry-A European Journal*, 2009, 15, 6116-6120.

20. K. J. Huang, Y. J. Liu and H. B. Wang, *Electrochimica Acta*, 2014, 118, 130-137.

21. D. Depan, T. C. Pesacreta and R. D. K. Misra, *Biomaterials Science*, 2014, 2, 264-274.

22. W. Sun, Y. Zhang and A. Hu, *Electroanalysis*, 2013, 25, 1417-1424.

23. M. J. A. Shiddiky, S. Rauf and P. H. Kithva, *Biosensors and Bioelectronics*, 2012, 35, 251-257.

24. Y. Wang, R. Yuan and Y. Chai, *Biosensors and Bioelectronics*, 2012, 38, 50-54.

25. W. Choi, J. Choi and J. H. Lee, *RSC Advances*, 2013, 3, 22455-22460.

26. L. Park, J. Kim and J. H. Lee, *Talanta*, 2013, 116, 736-742 .

27. C. Yang, Y. Wang and J. L. Marty, *Biosensors and Bioelectronics*, 2011, 26, 2724-2727.

28. S. Iijima, *Nature*, 1991, 354, 56-58.

29. X. J. Han, J. L. Tang, J. G. Wang and E. K. Wang, *Electrochimica Acta*, 2001, 46, 3367-3371.

30. G. Z. Liu, W. Q. Guo and D. D. Song, *Biosensors and Bioelectronics*, 2014, 52, 360-366.

31. L. Wang, X. Zheng and W. Zhang, *RSC Advances*, 2013, 3, 9042-9046.

32. K. Y. Hwa and B. Subramani, *Biosensors and Bioelectronics*, 2014, 62, 127 -133.

33. J. H. Chen, *Chem. Eng. Equip*, 2010, vol. 9, pp.1-2. (in Chinese)

34. W. S. Hummers Jr and R. E. Offeman, *Journal of the American Chemical Society*, 1958, 80, 1339-1339.

35. Y. Liu, R. Deng and Z. Wang, *Journal of Materials Chemistry*, 2012, 22, 13619-13624.

Analytical Methods Accepted Manuscript

36. N. Pan, D. Guan and Y. Yang, *Chemical Engineering Journal*, 2014, 236, 471-479.

37. A. Bonanni, C. K. Chua and M. Pumera, *Chemistry-A European Journal*, 2014, 20, 217-222.

38. X. Han, X. Fang and A. Shi, *Analytical biochemistry*, 2013, 443, 117-123.

39. Y. Hu, F. Li and X. Bai, *Chem. Commun.*, 2011, 47, 1743-1745.

40. P. Wipawakarn, H. Ju and D. K. Y. Wong, *Analytical and bioanalytical chemistry*, 2012, 402, 2817-2826.

41. K. Yang and C. Zhang, *Biosensors and Bioelectronics*, 2011, 28, 257-262.

42. M. L. Yola, T. Eren and N. Atar, *Electrochimica Acta*, 2014, 125, 38-47.

43. V. K. Gupta, M. L. Yola and M. S. Qureshi, *Sensors and Actuators B: Chemical*, 2013, 188, 1201-1211.

44. T. Yang, W. Zhang and M. Du, *Talanta*, 2008, 75, 987-994.

45. X. Zhang, F. Gao and X. L. Cai, *Materials Science and Engineering C*, 2013, 33, 3851-3857.